Adaptive tetrahedral subdivision for finite element analysis

Daniel Burkhart
Geometric Algorithms Group
Department of Computer Science
University of Kaiserslautern
67653 Kaiserslautern, Germany
Telephone: +49-631-205-3265
Fax: +49-631-205-3270
Email: burkhart@cs.uni-kl.de

Bernd Hamann
Institute for Data Analysis
and Visualization (IDAV)
Department of Computer Science
University of California, Davis
CA 95616-8562, U.S.A.
Email: hamann@cs.ucdavis.edu

Georg Umlauf
Computer Graphics Lab
Department of Computer Science
University of Applied Science Constance
78462 Constance, Germany
Email: umlauf@htwg-konstanz.de

***Abstract*—Realistic behavior of deformable objects is essential for many applications in computer graphics, engineering, or medicine. Typical techniques are either based on mass-spring-damper models, boundary element methods, finite difference methods, or finite element methods. These methods either lack accuracy or are computationally very expensive. If accuracy is required FEM computations use adaptive refinement, where regions with high gradients are refined locally. The bottleneck of this approach is still the gap between CAD and CAE representations.**

We present an approach to utilize solid subdivision for finite element simulations using an adaptive tetrahedral subdivision scheme based on $\sqrt{3}$ subdivision for triangular meshes. The advantage of this approach is the use of the subdivision representation the modeling, the visualization and the simulation of the solid model.

I. Introduction

Ordinary and partial differential equations arise in many computer graphics areas. Especially, physical simulation of deformable objects is essential for applications like computer animation, surgical training or mechanical engineering. While for surgical training real-time behavior is most critical, for computer animation and mechanical engineering realistic and physically accurate behavior are preferred.

In this paper, a method is presented using adaptive tetrahedral subdivision for finite element analysis. Until now, solid subdivision has only been applied to smooth deformations of objects. However, utilizing a solid subdivision has many advantages:

- *(i)* only one representation for modeling, visualization and simulation;
- *(ii)* implicit creation of well shaped, high quality meshes;
- *(iii)* level of detail and adaptivity;
- *(iv)* special features;
- *(v)* efficiency and stability;
- *(vi)* simple rules and data structures;
- *(vii)* arbitrary topology.

Our adaptive tetrahedral subdivision scheme is designed for efficient computations of finite element analysis. As our subdivision scheme supports sharp creases and corners, it is applicable to mechanical engineering. The advantage of our method against other refinement methods is that the boundary is a smooth subdivision surface. Hence, refining elements does not require communication between the CAE- and the CAD-system, because positions of new nodes are implicitly known.

II. Related Work

The four most common techniques for the simulation of deformable objects are mass-spring-damper (MSD) models [16], boundary element methods (BEM), finite difference methods (FDM), and finite element method (FEM). As MSD models are rather simple models, they are most likely to achieve real-time performance [15], [9]. The BEM have the best trade of between computational costs and physical accuracy [10], [8]. However, if accurate results are required, FDM and FEM have been used successfully for engineering applications[3]. To speed up the FEM computations adaptive refinements are used. Standard refinement methods like longest-edge bisection [13] have the drawback, that the boundary does not have a smooth limit surface.

While subdivision surfaces are popular in computer graphics and geometric modeling since their development in 1978[5], subdivision solids have gained less attention. One of the first algorithms was the generalization of Catmull-Clark surfaces to hexahedral solids [12]. As the topological refinement operation of this algorithm made it hard to analyze the smoothness of the resulting limit solid, Bajaj et al. [1] modified the operation to compute deformations that are provably smooth everywhere except at the vertices of the base mesh. Later, Chang et al. [6], [7] proposed a subdivision scheme for tetrahedral meshes based on trivariate box splines. The drawback of their approach are edge-bisections, which insert octahedra into the mesh. The resulting octahedra are then split along one of their diagonals into four tetrahedra. This choice of the diagonal can bias the resulting meshes towards a certain spatial direction. To remedy this effect Schaefer et al. [14] use a topological refinement that splits the octahedra symmetrically into eight tetrahedra and six octahedra. Their geometric smoothing allows for globally C^2-continuous deformations, except along edges of the base

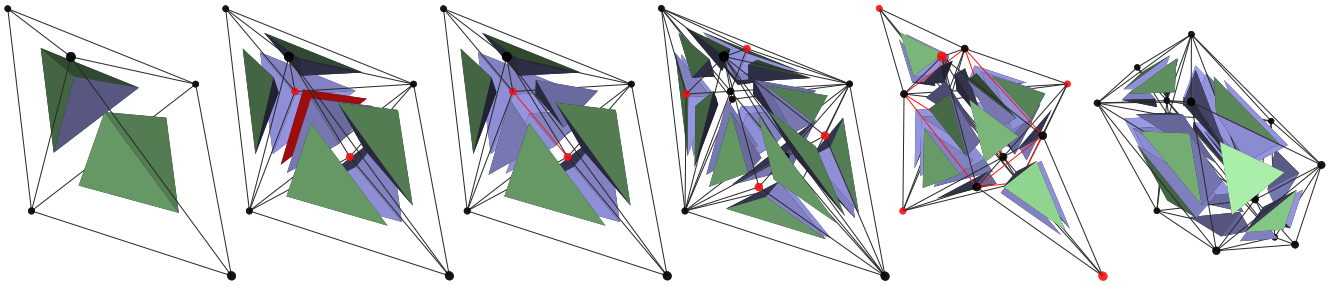

Fig. 1. An example for the tetrahedral subdivision scheme (left – right): base mesh, mesh after 1-4 splits, 2-3 flips, boundary 1-3 splits, boundary edge removals and optimization. Blue faces are interior faces, green faces are boundary faces.

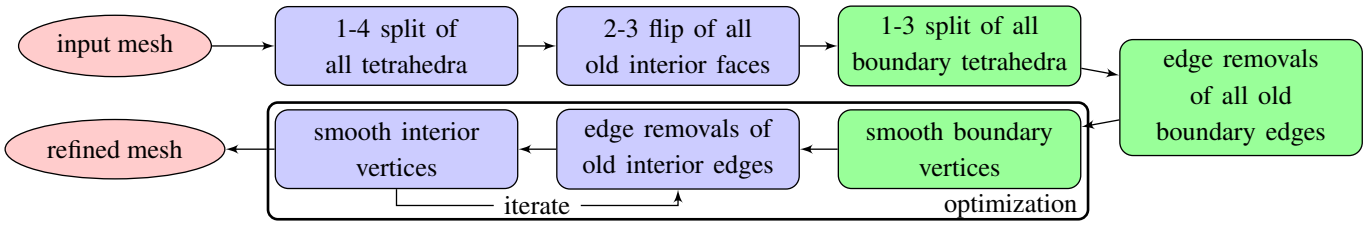

Fig. 2. The tetrahedral subdivision scheme. Blue and green shaded boxes represent interior and boundary operations, green shaded boxes represent boundary operations.

mesh. All these solid subdivision schemes are designed for 3d deformations and do not support adaptive refinement.

III. Adaptive, feature preserving tetrahedral subdivision

The subdivision scheme for tetrahedral meshes we use for the FEM simulation generalizes the idea of $\sqrt{3}$ subdivision [11] for triangular meshes, as it uses generalized split and flip operations [4]. While $\sqrt{3}$ subdivision is based on triangular 1-3 splits and edge flips, tetrahedral subdivision is based on tetrahedral 1-4 splits (Figure 3(a)) and edge removals (Figure 4(b)). Edge removals for two adjacent tetrahedra are called 2-3 flips (Figure 4). The subdivision process is a combination of 1-4 splits and 2-3 flips in the interior, the $\sqrt{3}$ scheme and edge removals on the boundary and optimization steps as shown in Figure 2. For these boundary steps, tetrahedral 1-3 splits (Figure 3(b)) are required. For preservation of sharp features 1-3 edge splits (Figure 3(c)) are required. The same sequence of operations is illustrated in Figure 1 for a simple base mesh of two tetrahedra. For details see [4].

In contrast to earlier solid subdivision schemes, this scheme allows for

- adaptive refinement by restricting the 2-3 flips and the boundary edge removals to the locally refined regions,
- control of the shape of the tetrahedra by adjusting the optimization steps, and
- preservation of sharp features by adjusting the two smoothing operations.

The latter can also be used to replace the original $\sqrt{3}$ smoothing by an interpolatory smoothing. These properties make this subdivision scheme suitable for FEM simulations.

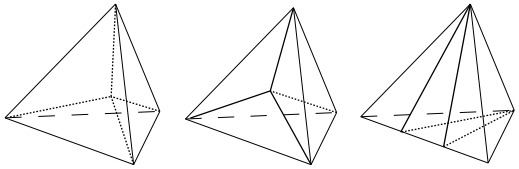

Fig. 3. Split operations for tetrahedral subdivision: a) 1-4 split, b) 1-3 split, c) 1-3 edge split.

IV. Finite element method

Most research that has applied FEM in animation and simulation has used linear finite elements [3]. To solve a continuum mechanical problem, the first step is to discretize the domain into a set of finite elements. However, the key to efficient and accurate solutions to these problems is not the quantity but also the quality of the elements. Thus, it is important to refine only in areas with large gradients, to keep the total number of elements small. This refinement requires adaptive meshing techniques, which must be combined with an appropriate error estimator, while at the same time the quality of the elements must be controlled. For this we use the tetrahedral subdivision scheme with optimization steps that maximize the minimal dihedral angles.

A. Linear elasticity

In linear elasticity a linear elastic solid model Ω consists of a set of nodes $\mathbf{x} = [x, y, z]^T$. These nodes are tetrahedalized to form the linear tetrahedral elements for the FE analysis. When forces are applied, Ω is deformed into a new shape. The corresponding displacement of $\mathbf{x}$ is defined as $\mathbf{u}(\mathbf{x}) = [u, v, w]^T$ moving $\mathbf{x}$ to $\mathbf{x} + \mathbf{u}$.

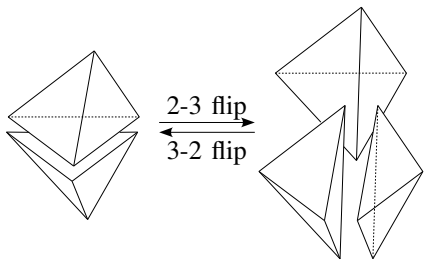

(a)

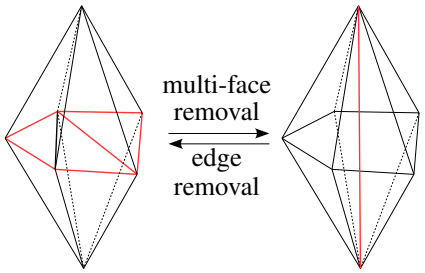

(b)

Fig. 4. Flip operation for tetrahedral subdivision.

The boundary of the domain Ω consists of the boundary Γ_1 with fixed displacements $\mathbf{u}(\mathbf{x}) = \mathbf{u_0}(\mathbf{x})$, the boundary Γ_2 where forces are applied, and the boundary Γ_3 without constraints. These components satisfy $\Gamma = \bigcup_i \Gamma_i$ and $\bigcap_i \Gamma_i = \emptyset$.

The strain energy of a linear elastic body Ω is

$$E_{\text{strain}} = \frac{1}{2} \int_\Omega \epsilon^T \sigma \, d\mathbf{x},$$

with the stress vector σ and the strain vector $\epsilon = [\epsilon_x \ \epsilon_y \ \epsilon_z \ \gamma_{xy} \ \gamma_{xz} \ \gamma_{yz}]^T$ defined as

$$\epsilon_x = \frac{\partial u}{\partial x}, \quad \epsilon_y = \frac{\partial u}{\partial y}, \quad \epsilon_z = \frac{\partial u}{\partial z},$$
$$\gamma_{xy} = \frac{\partial u}{\partial y} + \frac{\partial v}{\partial x}, \quad \gamma_{xz} = \frac{\partial u}{\partial z} + \frac{\partial w}{\partial x}, \quad \gamma_{yz} = \frac{\partial v}{\partial z} + \frac{\partial w}{\partial y}.$$

This can be rewritten as $\epsilon = Bu$, where B is called stress-displacement matrix.

$$B^T = \begin{bmatrix} \partial/\partial x & 0 & 0 & \partial/\partial y & \partial/\partial z & 0 \\ 0 & \partial/\partial y & 0 & \partial/\partial x & 0 & \partial/\partial z \\ 0 & 0 & \partial/\partial z & 0 & \partial/\partial x & \partial/\partial y \end{bmatrix}.$$

Now, Hook's law $\sigma = C\epsilon$ relates the stress vector σ to ϵ via the material matrix C. For homogeneous, isotropic material C is defined by the Lamé constants λ and μ

$$C = \begin{bmatrix} \lambda+2\mu & \lambda & \lambda & 0 & 0 & 0 \\ \lambda & \lambda+2\mu & \lambda & 0 & 0 & 0 \\ \lambda & \lambda & \lambda+2\mu & 0 & 0 & 0 \\ 0 & 0 & 0 & \mu & 0 & 0 \\ 0 & 0 & 0 & 0 & \mu & 0 \\ 0 & 0 & 0 & 0 & 0 & \mu \end{bmatrix}.$$

Rewriting the strain energy and adding work done by internal and external forces $\mathbf{f}$ and $\mathbf{g}$, respectively, yields the total energy function

$$E(\mathbf{u}) = \frac{1}{2} \int_\Omega \mathbf{u}^T B^T C B \, \mathbf{u} \, d\mathbf{x} - \int_\Omega \mathbf{f}^T \mathbf{u} \, d\mathbf{x} - \int_{\Gamma_1} \mathbf{g}^T d\mathbf{a}.$$

More details can be found in [3], [17].

B. Error indicator

To improve the accuracy of the FE solution the linear tetrahedral elements are refined. However, a refinement of the whole model is neither desirable nor necessary. It suffices to refine the model only in areas with a large approximation error. Hence, we require an a-posteriori error $\mathbf{e}$ that measures the difference between the exact solution $\mathbf{u}$ and an approximate solution $\hat{\mathbf{u}}$, i.e. $\mathbf{e} = \mathbf{u} - \hat{\mathbf{u}}$, see [2]. The error estimation we are using measures the approximation error for each tetrahedron by integrating the jump of the normal derivative of its faces.

V. Results

All our results were computed on a 2GHz Intel Core2 Duo with 4GB RAM using Getfem++.

To demonstrate the effectiveness of our method we show the simulation results for the engineering part shown in Figure 5 (top row) consisting of $2,799$ tetrahedra. To the top faces (yellow) of the tripod a vertical load is applied, i.e. this region is Γ_2 where the Neumann boundary conditions are applied. The bottom of the legs of the tripod is fixed, i.e. this region is Γ_1 with the Dirichlet boundary condition.

Figure 5 (second row) shows the deformed model. For the visualization of the normalized approximation error of the tetrahedra the color hue of the HSV model is linearly interpolated from $0°$ (low error) to $120°$ (high error). The simulation took 491ms while the average normalized error is 0.08. The histogram shows the error distribution for the tetrahedra.

For the next step the mesh regions with the largest error are selected and refined. These refined regions are highlighted in red in Figure 5 (third row). As some of these regions are isolated, we did one step of region growing to decrease the number of disconnected, refined regions. The adaptively refined mesh consists of $4,540$ tetrahedra. Figure 5 (fourth row) shows the deformation of this new tetrahedral mesh. The simulation took 596ms while the average normalized error is 0.03.

Figures 5 (fifth and sixth row) show a second step of adaptive subdivision and simulation. After the adaptive subdivision the mesh consists of $6,080$ tetrahedra. The simulation took 606ms while the average normalized error is 0.01.

Without adaptive refinement the mesh consists of $23,480$ tetrahedra after one subdivision step. This yields a simulation time of $7,574$ms with average normalized error 0.008 for the globally refined mesh.

The decrease of the average normalized error and the histograms getting narrower demonstrates that our method is effective. The efficiency of the proposed methods is demonstrated by comparing the computation times for the adaptively and the globally refined meshes.

VI. Conclusion and Future Work

In this paper we have presented an approach for combining solid subdivision and FE analysis. The major advantage of this

approach is that only one representation is used for modeling, visualization and simulation of solid models, by means of an adaptive tetrahedral subdivision tailored for FE applications. For the future we plan to combine this subdivision scheme with more complex FE models, e.g. non-linear deformations, and use the subdivision refineable functions for the FE simulation.

ACKNOWLEDGMENTS

This work was supported by the German Research Foundation (DFG) through an International Research Training Group (IRTG) grant, IRTG 1131, entitled "Visualization of Large and Unstructured Data sets", administered by the University of Kaiserslautern, Germany, and IDAV, University of California, Davis. Thanks to Klaus Denker for helping us with Figures 1 and 2.

REFERENCES

[1] C. Bajaj, S. Schaefer, J. Warren, and G. Xu. A subdivision scheme for hexahedral meshes. *The Visual Computer*, 18:343–356, 2002.

[2] R.E. Bank and A. Weiser. Some a posteriori error estimators for elliptic partial differential equations. *Mathematics of Computation*, 44:283–301, 1985.

[3] M. Bro-Nielsen. Surgery simulation using fast finite elements. In *Proc. 4th Int. Conf. on Vis. in Biomed. Comp.*, 1996.

[4] D. Burkhart, B. Hamann, and G. Umlauf. Adaptive and feature-preserving subdivision for high-quality tetrahedral meshes. *Comput. Graph. Forum*, 29(1):117–127, 2010.

[5] E. Catmull and J. Clark. Recursively generated b-spline surfaces on arbitrary topological meshes. *Computer-Aided Design*, 10(6):350–355, 1978.

[6] Y. Chang, K. Mcdonnell, and H. Qin. A new solid subdivision scheme based on box splines. In *Proc. Solid Modeling*, pages 226–233, 2002.

[7] Y. Chang, K. Mcdonnell, and H. Qin. An interpolatory subdivision for volumetric models over simplicial complexes. In *Proc. Shape Modeling Intl.*, pages 143–152, 2003.

[8] S. Cotin, H. Delingette, and N. Ayache. Real-time elastic deformations of soft tissues for surgery simulation. *IEEE TVCG*, 5(1):62–73, 1999.

[9] M. Desbrun, P. Schröder, and A. Barr. Interactive animation of structured deformable objects. In *Proc. of Conf. on Graphics Interface*, pages 1–8. Morgan Kaufmann, 1999.

[10] D.L. James and D.K. Pai. Artdefo: accurate real time deformable objects. *SIGGR.*, pages 65–72, 1999.

[11] L. Kobbelt. $\sqrt{3}$ subdivision. *SIGGR.*, pages 103–112, 2000.

[12] R. MacCracken and K. Joy. Free-form deformations with lattices of arbitrary topology. *SIGGR.*, pages 181–188, 1996.

[13] T. Roxborough and G.M. Nielson. Tetrahedron based, least squares, progressive volume models with application to freehand ultrasound data. In *Proc. of Conf. on Visualization*, pages 93–100, 2000.

[14] S. Schaefer, J. Hakenberg, and J. Warren. Smooth subdivision of tetrahedral meshes. In *Symp. on Geometry Processing*, pages 147–154, 2004.

[15] D. Terzopoulos, J. Platt, A. Barr, and K. Fleischer. Elastically deformable models. *SIGGR.*, pages 205–214, 1987.

[16] X. Wu, M.S. Downes, T. Goktekin, and F. Tendick. Adaptive nonlinear finite elements for deformable body simulation using dynamic progressive meshes. *Comput. Graph. Forum*, 20(3), 2001.

[17] O.C. Zienkiewicz and R.L. Taylor. *The Finite Element Method, Volume 1+2*. Butterworth, 5th edition, 2000.

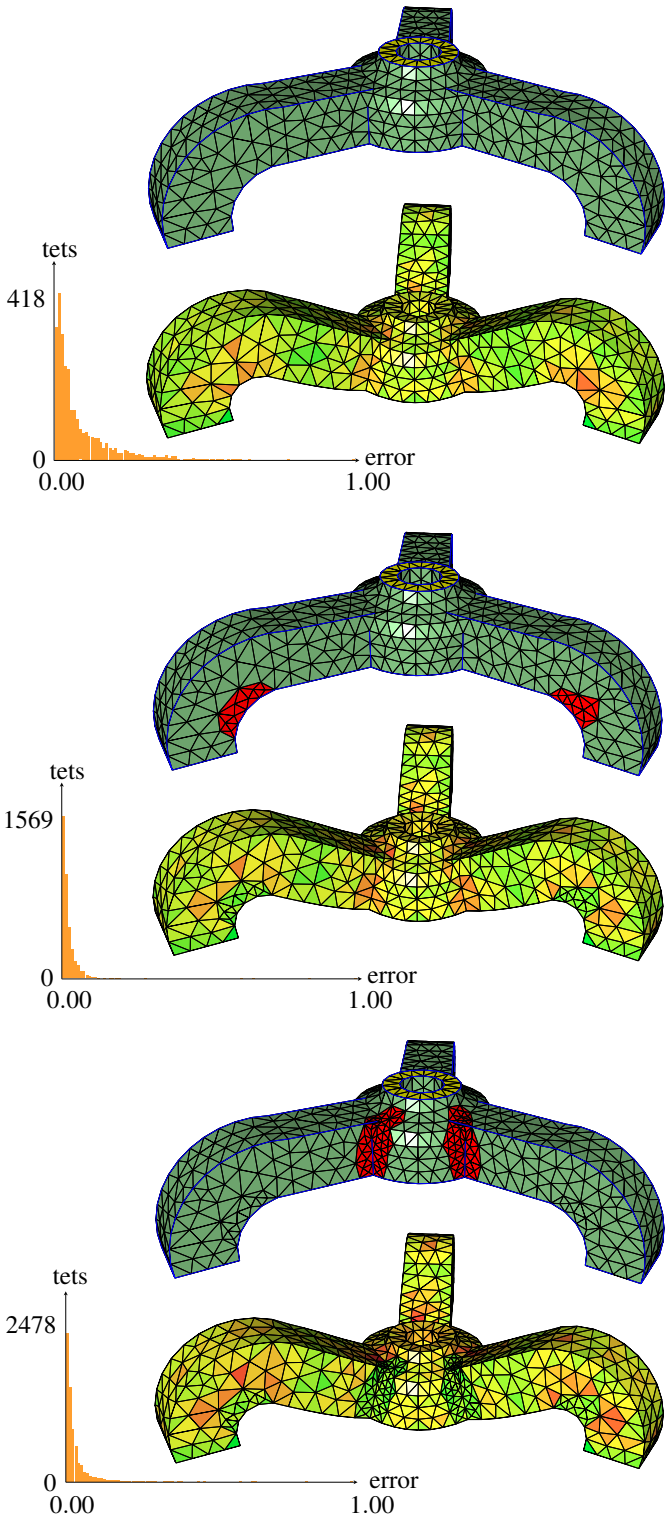

Fig. 5. Two rounds of adaptive subdivision and FE simulation (top – bottom): tetrahedral base mesh ($2,799$ tetrahedra), simulation result with visualization of the normalized approximation error (green=low – red=high) and the histogram of the error distribution, adaptively refined mesh ($4,540$ tetrahedra) showing the refined regions in red, simulation results for the once refined mesh, twice adaptively refined mesh ($6,080$ tetrahedra), simulation results for the twice refined mesh.